Photoinduced switching to metallic states in the two-dimensional organic Mott insulator dimethylphenazine-tetrafluorotetracyanoquinodimethane with anisotropic molecular stacks

Hiroyuki Matsuzaki,[1] Masa-aki Ohkura,[2] Yu Ishige,[2] Yoshio Nogami,[3] and Hiroshi Okamoto[2]

[1]*Research Institute of Instrumentation Frontier, National Institute of Advanced Industrial Science and Technology (AIST), Tsukuba Central 2, 1-1-1 Umezono, Tsukuba, Ibaraki 305-8568, Japan*

[2]*Department of Advanced Materials Science, Graduate School of Frontier Sciences, University of Tokyo, 5-1-5 Kashiwanoha, Kashiwa, Chiba 277-8561, Japan*

[3]*Department of Physics, Faculty of Science, Okayama University, Tsushima-naka 3-1-1, Okayama 700-8530, Japan*

(Received 14 December 2014; revised manuscript received 30 May 2015; published 18 June 2015)

A photoinduced phase transition was investigated in an organic charge-transfer (CT) complex M_2P-$TCNQF_4$, [M_2P: 5,10-dihydro-5,10-dimethylphenazine, donor (D) molecule; $TCNQF_4$: 2,3,5,6-tetrafluoro-7,7,8,8-tetracyanoquinodimethane, acceptor (A) molecule] by means of femtosecond pump-probe reflection spectroscopy. This is an ionic compound and has a peculiar two-dimensional (2D) molecular arrangement; the same A (or D) molecules arrange along the [100] direction, and A and D molecules alternately arrange along the [111] direction. It results in a strongly anisotropic two-dimensional electronic structure. This compound shows a structural and magnetic phase transition at 122 K below which the two neighboring molecules are dimerized along both the [100] and [111] directions. We demonstrate that two kinds of photoinduced phase transitions occur by irradiation of a femtosecond laser pulse; in the high-temperature lattice-uniform phase, a quasi-one-dimensional (1D) metallic state along the AA(DD) stack is generated, and in the low-temperature lattice-dimerized phase, a quasi-2D metallic state is initially produced and molecular dimerizations are subsequently released. Mixed-stack CT compounds consisting of DA stacks are generally insulators or semiconductors in the ground state. Here, such a dynamical metallization in the DA stack is demonstrated. The release of the dimerizations drives several kinds of coherent oscillations which play an important role in the stabilization of the lattice-dimerized phase. The mechanisms of those photoinduced phase transitions are discussed in terms of the magnitudes of the anisotropic bandwidths and molecular dimerizations along two different directions of the molecular stacks.

DOI: 10.1103/PhysRevB.91.245140 PACS number(s): 71.30.+h, 75.30.Fv, 78.40.Me, 78.47.J−

I. INTRODUCTION

State-of-art ultrafast laser technology has opened up new possibilities for ultrafast control of the electronic properties and crystal structures of solids by irradiation of a femtosecond laser pulse. Such a photocontrol can be achieved via a phase change in a solid by light, which is called a photoinduced phase transition (PIPT) [1–5]. PIPTs are attracting much attention in the fields of condensed-matter physics and chemistry from the viewpoints of material science, nonequilibrium physics, as well as of applications to future optical switching and memory devices.

To realize such ultrafast PIPTs, low-dimensional organic molecular compounds are promising candidates. They have strong instabilities inherent to both electron correlation and electron (spin)-lattice interactions, and sometimes exhibit characteristic phase transitions by lowering the temperature and/or applying pressure. A photoexcitation can stimulate such instabilities and ultrafast PIPTs are expected to be driven. Actually, various ultrafast PIPT phenomena have been observed in this class of organic molecular compounds [6–20].

In the present study, we focus on an organic charge-transfer (CT) compound, M_2P-$TCNQF_4$ (M_2P: 5,10-dihydro-5,10-dimethylphenazine; $TCNQF_4$: 2,3,5,6-tetrafluoro-7,7,8,8-tetracyanoquinodimethane). The molecular structures of M_2P and $TCNQF_4$ are shown in Fig. 1(a). This compound is an ionic compound in which the degree of CT from donor (D) to acceptor (A) molecules ρ is very close to 1 [21–23]. Figure 1(b) shows the crystal structure of M_2P-$TCNQF_4$ at 294 K viewed perpendicular to the $(01\bar{1})$ plane. D and A molecules stack alternately along the [111] direction. As seen in Fig. 1(b), D molecules and A molecules also stack along the [100] direction, respectively, forming two-dimensional (2D) molecular arrangements. Hereafter, we refer to the [111] and [100] directions as the DA stack direction and the AA(DD) stack direction, respectively. According to the calculation of the transfer integrals between neighboring molecules (t_{DD}, t_{AA}, and t_{DA}) [24,25], there are finite CT interactions along the DD and AA stacks as well as the DA stacks ($t_{DD} = 29.3$ meV, $t_{AA} = 43.1$ meV, and $t_{DA} = 67.1$ meV). The transfer integrals t_{DD}, t_{AA}, and t_{DA} were estimated by using the extended Hückel molecular orbital calculations (see Ref. [24] for details). Moreover, the overlap of π orbitals along the normal to the 2D sheets is very small so that the intermolecular interaction between the neighboring 2D molecular sheets can be neglected. Thus, the anisotropic 2D electronic structure is formed in M_2P-$TCNQF_4$.

By lowering the temperature from 294 K, M_2P-$TCNQF_4$ exhibits a structural transition at $T_C \sim 122$ K, below which the D and A molecules show displacements and the magnetic (spin) susceptibility sharply decreases, as shown in Fig. 2(a) [21]. The crystal structure below T_C (at 25 K) is shown in Fig. 1(c). Note that directions and planes are indexed using the original lattice in the high-temperature phase even below T_C for ease in discussing the temperature variations of the crystal structure. At 25 K, the D and A molecules shift, as shown by the yellow and red arrows in Fig. 1(b), resulting in dimerization of the neighboring DD molecules and AA molecules. In Fig. 1(b), the lengths of the arrows were normalized to an appropriate scale so that the directions

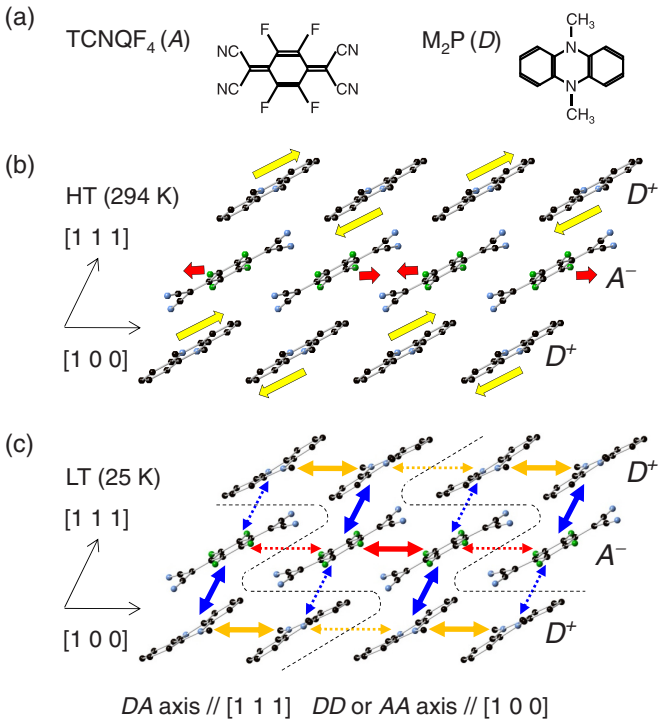

FIG. 1. (Color online) (a) Molecular structures of M_2P and $TCNQF_4$. Crystal structures of M_2P-$TCNQF_4$ viewed perpendicular to a $(01\bar{1})$ plane at (b) 294 K and (c) 25 K. The directions of the axes were indexed using the original lattice. Yellow and red arrows in (b) show molecular displacements at 25 K of M_2P and $TCNQF_4$, respectively. Solid and dashed arrows in (c) show intradimer and interdimer spacing, respectively. Dashed lines indicate the spatial pattern of molecular dimerizations.

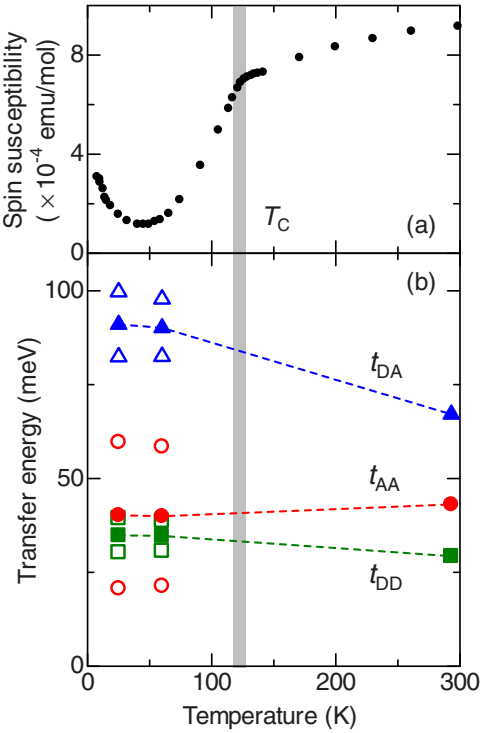

FIG. 2. (Color online) Temperature variations of (a) spin susceptibility (taken from Ref. [21]) and (b) transfer energies in M_2P-$TCNQF_4$. A vertical bar shows the phase transition temperature T_C. In (b), open marks below T_C show the intradimer transfer energy t_1 (higher value) and interdimer transfer energy t_2 (lower value) and solid marks show the averaged values of t_1 and t_2.

and relative magnitudes of the molecular displacements can be clearly seen. These molecular displacements also lead to dimerizations of the neighboring D and A molecules along the DA stacks. In Fig. 2(b), we plot the intradimer transfer integrals t_1 and interdimer transfer integrals t_2 (open symbols) as well as their averages (solid symbols) for the DD, AA, and DA stacks at three temperatures (294, 60, and 25 K). The pattern of molecular displacements in the low-temperature phase is quite unique, and a spin-singlet state is formed in each DA dimer via such displacements of both D and A molecules below T_C.

Thus, M_2P-$TCNQF_4$ has uniform AA and DD stacks as does tetrathiafulvalene-tetracyanoquinodimethane (TTF-TCNQ) [26] in the high-temperature phase. Because of $\rho \approx 1$, however, it is an anisotropic 2D Mott insulator. By utilizing the finite CT interaction along the DA stack, it can be expected that a metallic behavior would be generated via charge transfers between M_2P and $TCNQF_4$ induced by photoexcitation of an A^- to D^+ transition. Recently, Mott insulator to metal transitions by irradiation of a femtosecond laser pulse have been found in one-dimensional (1D) systems of halogen-bridged transition metal compounds, $[Ni(chxn)_2Br]Br_2$ [27] and $[Pd(en)_2Br](C_5\text{-}Y)_2 \cdot H_2O$ [28], an organic molecular compound, ET-F_2TCNQ [bis(ethylenedithio)tetrathiafulvalene-difluorotetracyanoquinodimethane] [14], and 2D systems of layered cuprate compounds, Nd_2CuO_4 and La_2CuO_4 [29,30]. It is an intriguing subject to investigate the possibilities of whether an anisotropic Mott insulator is photoconverted to a 1D metal or a 2D one, or, equivalently, whether or not a metallic state is formed along the DA stacks. In the low-temperature lattice-dimerized phase, on the other hand, photocarriers will be able to stimulate the instability of the spin-lattice system through the breaking of spin-singlet states, and then melting of the lattice-dimerized phase by photoirradiation is expected to occur, as observed in alkali (M)-TCNQ ($M = K$, Na, and Rb) [16–19] and a neutral radical crystal, trithiatriazapentalenyl (TTTA) [31]. In addition, a metallic state might also be photogenerated. It is also an important subject to clarify these phenomena.

On the basis of these considerations, in this paper, we report on the photoinduced phase transition of an M_2P-$TCNQF_4$ single crystal with a peculiar 2D electronic structure investigated by femtosecond (fs) pump-probe (PP) reflection spectroscopy, and discuss the nature of the photoinduced phase transition based on optical reflection and Raman spectroscopies as well as ultrafast laser spectroscopy. The contents of this paper is as follows. In Sec. II, we detail the experimental procedures. We present the experimental results and their discussions in Secs. III and IV, respectively. In Sec. V, we summarize the present study.

II. EXPERIMENTAL DETAILS

Single crystals of M_2P-$TCNQF_4$ were grown by a previously reported recrystallization method [21]. The typical

crystal size was about $0.6 \times 0.6 \times 0.3\,\mathrm{mm}^3$. Polarized Raman spectra were measured by using a Raman spectrometer in a backscattering configuration. The spectrometer was equipped with an optical microscope. A He-Ne laser (1.96 eV) was used as the light source.

Femtosecond pump-probe (PP) reflection spectroscopy was conducted using a Ti : Al_2O_3 regenerative amplifier as the light source. The output from the regenerative amplifier (photon energy of 1.55 eV, a pulse width of 130 fs, and a repetition rate of 1 kHz) was separated into two beams for the excitation of two optical parametric amplifiers (OPAs). Pump (0.96 eV) and probe (0.1−2.0 eV) pulses were obtained from the two OPAs. The delay time t_d of the probe pulse relative to the pump pulse was controlled by changing the path length of the pump pulse. The temporal resolution of the system was ca. 180 fs. The excitation photon density x_{ph} was evaluated from an equation $x_{\mathrm{ph}} = I_p(1 - R_p)(1 - 1/e)/l_p$. Here, I_p, l_p, and R_p are the excitation photon density per unit area, the absorption depth, and the reflection loss of the pump light, respectively. For the above-mentioned optical spectroscopies, we used a specially designed and vibration-reduced conduction-type cryostat in the low-temperature measurements.

III. EXPERIMENTAL RESULTS

A. Photoinduced change of reflectivity and dielectric function at high-temperature phase (294 K)

The steady-state optical spectra of M_2P-$TCNQF_4$ were previously reported in Ref. [25] by the present authors. Figures 3(a) and 3(b) [Figs. 5(a) and 5(b)] show the polarized reflectivity (R) spectra at 294 K (10 K) with electric fields of light E parallel to (∥) the DA stacks and AA(DD) stacks, respectively, which were measured on a $(01\bar{1})$ plane. The imaginary part of the dielectric constants (ε_2) for $E \parallel$ DA and $E \parallel$ AA(DD) are depicted in Figs. 4(a) and 4(b) (294 K) and in Figs. 6(a) and 6(b) (10 K) by dashed lines, respectively.

In this section, we discuss the photoresponses at 294 K. Before the discussions of the results, we summarize the assignments of the optical absorptions observed at 294 K [25]. The peak structures at 0.9 eV for $E \parallel$ DA labeled b [the dashed line in Fig. 4(a)] and at 0.77 eV for $E \parallel$ AA(DD) labeled a [the dashed line in Fig. 4(b)] can be attributed to the A^- to D^+ transition (CT transition) and the Mott-gap transition from A^- to A^-, respectively. The peak structure labeled c at 1.37 eV [the dashed line in Fig. 4(b)] can be assigned to the D^+ to D^+ transition.

In Figs. 3(c) and 3(d), we show the spectra of photoinduced reflectivity changes ΔR at 294 K for typical delay times t_d. The pump light has an energy (E_{pump}) of 0.96 eV and is polarized parallel to the DA stack, which gives rise to the excitation of the A^- to D^+ transition. The absorption depth of the pump light is estimated to be 82 nm. The probe light is set to be polarized parallel to the DA stack [Fig. 3(a)] and the AA(DD) stack [Fig. 3(b)] to investigate the photoinduced change of the anisotropic 2D electronic structure. The excitation photon density x_{ph} is 0.38 photon (ph)/DA pair. Immediately after the photoexcitation ($t_d = 0.1$ ps), the R in the mid-IR region below ∼0.4 eV monotonically increases with a decrease in energy, while the R decreases over a wide energy region at

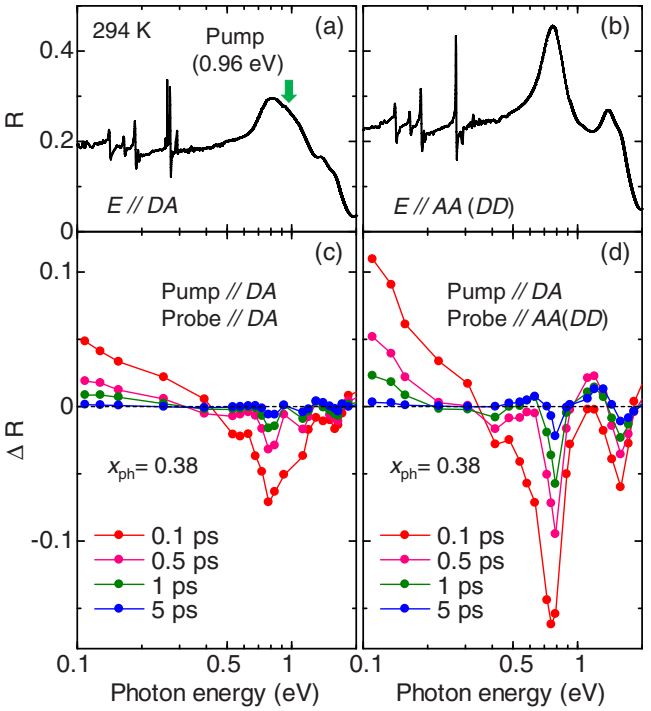

FIG. 3. (Color online) Polarized reflectivity spectra of M_2P-$TCNQF_4$ on a $(01\bar{1})$ plane with the electric fields of light E parallel to (∥) (a) the DA stack and (b) the AA(DD) stack at 294 K. Photoinduced reflectivity changes (ΔR) spectra for a typical delay time t_d with the electric field of the probe light E_{pr} parallel to (∥) (c) the DA stack and (d) the AA(DD) stack at 294 K. The photon energy and polarization of the pump light is 0.96 eV [the solid arrows in (a)] and is parallel to the DA stack, respectively. The excitation density of the pump light is 0.38 photon/DA pair.

0.4−2 eV due to photobleaching of the original optical transition, for both polarizations of the probe light [$E \parallel$ DA and $E \parallel$ AA(DD)]. As can be seen, the reflectivity changes for $E \parallel$ DA [Fig. 3(c)] are small as compared to those for $E \parallel$ AA(DD) [Fig. 3(d)]; ΔR at 0.11 eV reaches 0.11 in $E \parallel$ AA(DD), while

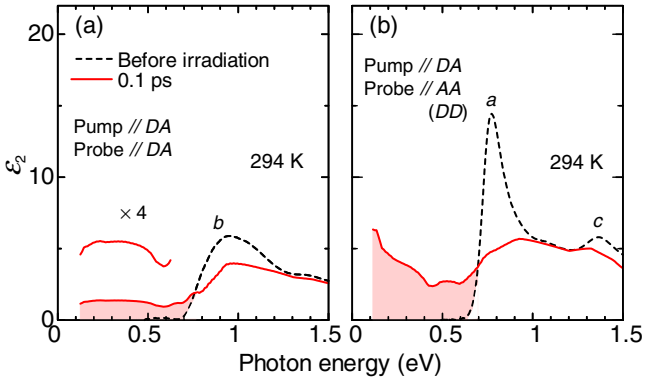

FIG. 4. (Color online) Transient spectra ($t_d = 0.1$ ps) of the imaginary part of dielectric constants (ε_2) (solid lines) for (a) the DA stack and (b) the AA(DD) stack at 294 K. The dashed lines represent the steady-state polarized ε_2 spectra (before irradiation). Shaded areas show the photoinduced ε_2 spectra transferred to the inner-gap region.

it reaches 0.05 in $E \parallel$ DA for $x_{ph} = 0.38$ ph/DA pair. [$\Delta R/R$ at 0.11 eV reaches 0.5 in $E \parallel$ AA(DD), while it reaches 0.25 in $E \parallel$ DA for $x_{ph} = 0.38$ ph/DA pair.]

To get quantitative information on the photoinduced phase, the photoinduced change in ε_2 was calculated by a Kramers-Kronig transformation of $R + \Delta R$. The transient ε_2 spectra at $t_d = 0.1$ ps for $E \parallel$ DA and $E \parallel$ AA(DD) are presented by the solid lines in Figs. 4(a) and 4(b), respectively. As can be seen in Fig. 4(b), the ε_2 for $E \parallel$ AA(DD) gradually increases with lowering the photon energy to 0.10 eV and the spectral intensity of the A^- to A^- transition is largely decreased, suggesting the closing of the optical gap due to the formation of a metallic state along the AA(DD) stack. For $E \parallel$ DA [Fig. 4(a)], in contrast, the ε_2 has a much smaller spectral weight in the inner-gap region compared to that for $E \parallel$ AA(DD). In fact, the calculated ratio of integrated ε_2 intensity induced in the inner-gap region to that of the original optical transition (0.5−1.25 eV) is 0.27 for $E \parallel$ DA, which is much smaller than that (0.47) for $E \parallel$ AA(DD). In Fig. 4(a), we show a magnified view of ε_2 below 0.6 eV to further scrutinize the spectral changes. For $E \parallel$ DA, the ε_2 spectrum exhibits a broad midgap absorption with a broad peak at around ∼0.3 eV, which differs considerably from the results of $E \parallel$ AA(DD) shown in Fig. 4(b). From these results, we can conclude that photogenerated carriers are less conductive along the DA stack and a quasi-1D transient metallic state is photogenerated along the AA(DD) stack at 294 K.

B. Photoinduced change of reflectivity and dielectric function at low-temperature phase (10 K)

To investigate how the photoexcited state of M_2P-$TCNQF_4$ varies depending on the crystal and electronic structures of the ground state, we measured the photoinduced reflectivity changes in the low-temperature phase. In this section, we report their results.

Before the detailed discussions, we comment on several features of the ε_2 spectra at 10 K [dashed lines in Figs. 6(a) and (b)], which are not observed at 294 K [dashed lines in Figs. 4(a) and (b)]. The ε_2 spectrum for $E \parallel$ DA shown in Fig. 6(a) includes the finite components of the A^- to A^- transition (band a) polarized parallel to the AA(DD) stack. It is because the DA stack is not perpendicular to the AA(DD) stack. In addition, in the ε_2 spectrum for $E \parallel$ DA [Fig. 6(a)], a shoulder structure can be discriminated at about 0.20 eV higher than the peak energy of the A^- to D^+ transition (band b). It can be attributed to the phonon sideband related to the intramolecular vibrational mode of the M_2P molecule [25].

The ΔR spectra due to the excitation of the A^- to D^+ transition ($E_{pump} = 0.96$ eV) for typical delay times t_d are shown in Figs. 5(c) and 5(d). The polarization, photon energy, and excitation photon density of the pump light are the same as those in the measurements at 294 K. The absorption depth of the pump light is estimated to be 46 nm. The polarization of the probe light is also the same as that at 294 K. The overall feature in the spectral shape of ΔR for $t_d = 0.1$ ps can be understood in an analogous way as at 294 K: the photoinduced decrease of ΔR at 0.4−2 eV due to the bleaching of the original optical transition and the gradual increase of ΔR below ∼0.4 eV with a decrease in photon energy for both polarizations of the probe

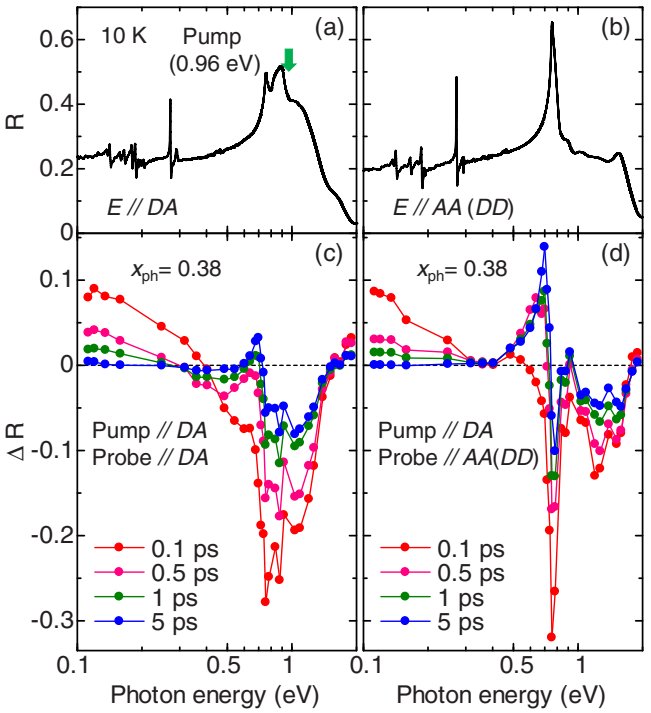

FIG. 5. (Color online) Polarized reflectivity spectra of M_2P-$TCNQF_4$ on a $(01\bar{1})$ plane with the electric fields of light E parallel to (∥) (a) the DA stack and (b) the AA(DD) stack at 10 K. Photoinduced reflectivity changes (ΔR) spectra for a typical delay time t_d with the electric field of the probe light E_{pr} parallel to (∥) (c) the DA stack and (d) the AA(DD) stack at 10 K. The photon energy and polarization of the pump light is 0.96 eV [the solid arrows in (a)] and is parallel to the DA stack, respectively. The excitation density of the pump light is 0.38 photon/DA pair.

light [$E \parallel$ DA and $E \parallel$ AA(DD)]. As shown in Fig. 5(c), for $E \parallel$ DA, the reflectivity change below 0.4 eV at 10 K is much more enhanced as compared to that at 294 K, even though the original value of reflectivity is almost the same ($R \sim 0.19$ at 294 K and $R \sim 0.23$ at 10 K below 0.4 eV). In fact, ΔR at 0.11 eV for $E \parallel$ DA reaches 0.095 at 10 K, while it reaches 0.05 at 294 K. The transient ε_2 spectra at $t_d = 0.1$ ps and at 10 K, for $E \parallel$ DA and $E \parallel$ AA(DD), are presented by the solid lines in Figs. 6(a) and 6(b), respectively. For both polarizations, the ε_2 gradually increases with lowering the photon energy down to 0.10 eV, and the spectral intensities of the D^+ to A^- transition and the A^- to A^- transition are considerably decreased. It suggests that the optical gaps are closed along the DA stack as well as along the AA(DD) stack, and the quasi-2D metallic state is transiently generated by the photoexcitation. This result is a contrast to the result at 294 K, in which a quasi-1D metallic state is photogenerated, as shown in Figs. 4(a) and 4(b).

As seen in Fig. 5(d), the ΔR spectra for $E \parallel$ AA(DD) at 10 K exhibits a characteristic time dependence of the spectral shapes in the energy region from 0.6 to 1.0 eV, which originates from the spectral change of the A^- to A^- transition. Just after the photoirradiation ($t_d = 0.1$ ps), ΔR is negative for the whole energy region of the A^- to A^- transition (0.6−1.0 eV), which is due to the bleaching of the optical transition by photocarrier generation. At $t_d = 0.5$ ps,

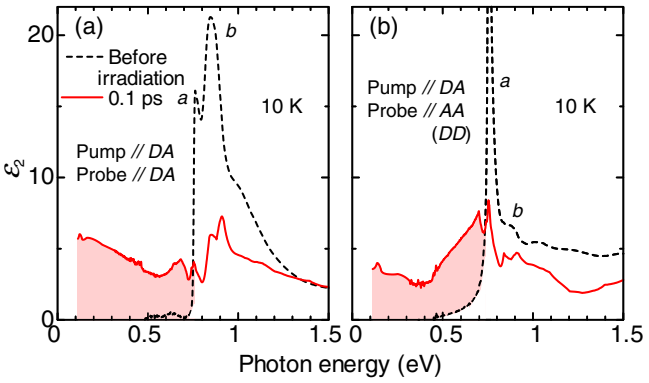

FIG. 6. (Color online) Transient spectra ($t_d = 0.1$ ps) of the imaginary part of dielectric constants (ε_2) (solid lines) for (a) the DA stack and (b) the AA(DD) stack at 10 K. The dashed lines represent the steady-state polarized ε_2 spectra (before irradiation). Shaded areas show the photoinduced ε_2 spectra transferred to the inner-gap region.

however, ΔR becomes positive in the lower-energy region at 0.6−0.75 eV. To see such spectral changes more clearly, expanded $\Delta R/R$ spectra for typical delay times are shown in Fig. 7(b). The spectral change of $\Delta R/R$ at $t_d = 0.5$ ps is analogous to the calculated differential R spectra $[R(\omega - \delta\omega) - R(\omega)]/R(\omega)$ ($\delta\omega = 10, 20$, and 30 meV), shown in Fig. 7(a). This suggests that photocarriers induce a redshift of the A^- to A^- transition within 0.5 ps.

In M_2P-$TCNQF_4$, the peak energy of the A^- to A^- transition is strongly correlated with the degree of molecular dimerization. In Fig. 7(c), the temperature dependence of the energy position of the A^- to A^- transition (E_{AA}) is shown by the solid circles [25]; E_{AA} gradually decreases as the temperature is increased. This temperature dependence of E_{AA} is in good agreement with that of the IR intensity of the intramolecular vibration (a_g) mode I_d, which is a crude measure of the dimeric molecular displacements associated with the structural phase transition [open circles in Fig. 7(c)] [25]. Such a close correlation suggests that the transient redshift of the A^- to A^- transition can be attributed to the photoinduced decrease of the dimeric molecular displacements. The magnitude of the peak-energy shift in E_{AA} ($\sim$ 30−40 meV) by photoirradiation is comparable to the magnitude of the peak-energy shift from 10 to 150 K (above T_C). Thus, the spectral change after 0.5 ps shows that the dimeric molecular displacements are largely released by photoirradiation within 0.5 ps. Namely, ultrafast photoinduced melting of the lattice-dimerized phase occurs at 10 K.

IV. DISCUSSION

A. Dynamical aspects of photoinduced phase transitions

In this section, we discuss the dynamical aspects of the photoinduced phase transition observed in the high-temperature phase (294 K) and in the low-temperature phase (10 K). $\Delta R/R$ at 0.13 eV for $E \parallel$ AA and $E \parallel$ DA characterizes photogeneration and the decay of transient metallic states at each temperature (294 and 10 K). $\Delta R/R$ at 0.70 eV for $E \parallel$ AA (10 K) characterizes the redshift of the A^- to

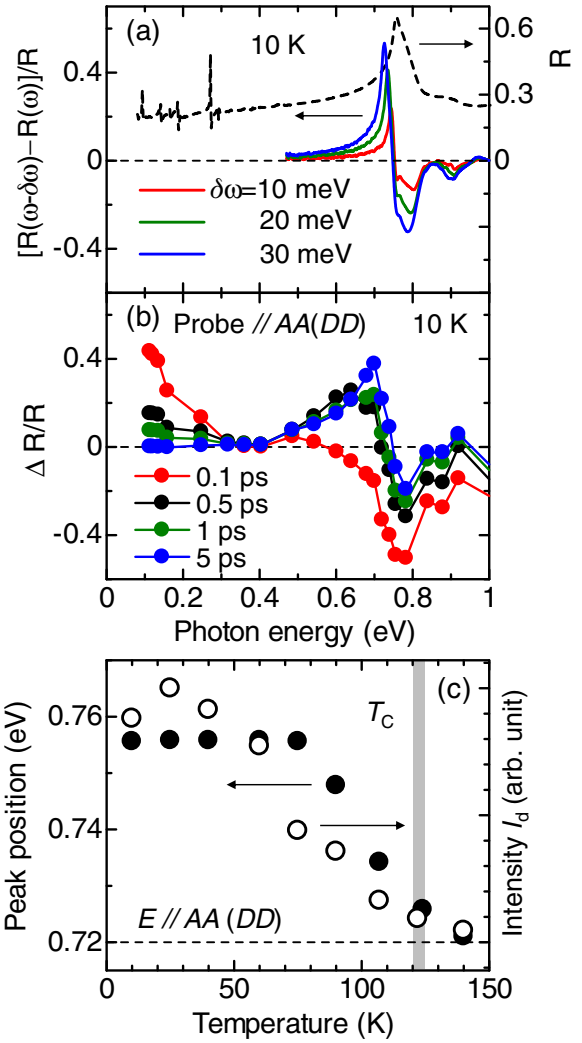

FIG. 7. (Color online) (a) The dashed line shows the expanded polarized reflectivity (below 1 eV) for $E \parallel$ AA(DD) at 10 K. Calculated differential reflectivity $\{[R(\omega - \delta\omega) - R(\omega)]/R(\omega)\}$ spectra for $\delta\omega = 10$, 20, 30 meV (solid lines). (b) Expanded $\Delta R/R$ spectra of $E_{pr} \parallel$ AA(DD) for a typical delay time t_d. (c) Temperature dependence of the peak energy of band a (the Mott-gap transition from A^- to A^-) (solid circles) and the intensity I_d of the IR active a_g mode at around 1450 cm^{-1} of M_2P-$TCNQF_4$ (open circles) [25]. A vertical bar shows the phase transition temperature T_C.

A^- transition and therefore directly reflects the photoinduced release of the dimerization in the low-temperature phase.

Figures 8(a), 8(b), and 8(d) show the time profiles for $\Delta R/R$ at 0.13 eV for $E \parallel$ AA and $E \parallel$ DA (294 and 10 K), and at 0.70 eV for $E \parallel$ AA (10 K) by the solid circles. $\Delta R/R$ at 0.13 eV rises up within the time resolution. It recovers within 1 ps at both 294 and 10 K, indicating that the decay time of photoinduced metallic states is very short, being independent of the degree in the anisotropy of the electronic structure and the dimerization. $\Delta R/R$ at 0.70 eV also decreases within the time resolution, which is the bleaching of the A^- to A^- transition due to the photogeneration of the metallic state. In this process, the molecular dimerizations will not be changed, since the periods of the lattice phonons corresponding to the dimerization in this type of organic molecular compound are

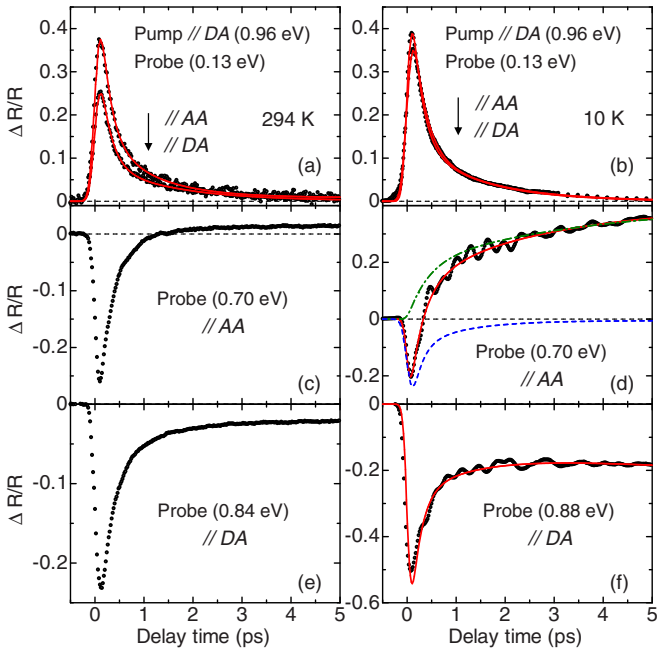

FIG. 8. (Color online) Time profiles of $\Delta R/R$ for (a) 0.13 eV ($E_{pr} \parallel$ AA and DA), (c) 0.70 eV ($E_{pr} \parallel$ AA), and (e) 0.84 eV ($E_{pr} \parallel$ DA) at 294 K (open circles). Time profiles of $\Delta R/R$ for (b) 0.13 eV ($E_{pr} \parallel$ AA and DA), (d) 0.70 eV ($E_{pr} \parallel$ AA), and (f) 0.88 eV ($E_{pr} \parallel$ DA) at 10 K (open circles). The solid lines in (a), (b), (d), and (f) show the fitting curves. In (d), the dashed line and dashed-dotted line correspond to the first and second terms in Eq. (2), respectively (see text).

TABLE I. Time constants (τ_i) and corresponding amplitudes (A_i, B_i) of time profiles $\Delta R/R$ [Figs. 8(a), 8(b), 8(d), and 8(f)] measured for 0.13 eV ($E_{pr} \parallel$ AA and DA) at 294 K, and for 0.13 eV ($E_{pr} \parallel$ AA and DA), 0.70 eV ($E_{pr} \parallel$ AA), and (e) 0.88 eV ($E_{pr} \parallel$ DA) at 10 K. Bleach and rise correspond to the component expressed by the first and second terms in Eq. (2), respectively (see text).

		i		
294 K		0	1	2
0.13 eV	A_i (%)	1.2	73.6	25.2
$\parallel$ AA	τ_i (ps)		0.19	0.99
0.13 eV	A_i (%)	0.2	79.4	20.4
$\parallel$ DA	τ_i (ps)		0.21	1.47
10 K		0	1	2
0.13 eV	A_i (%)	0.5	78.2	21.3
$\parallel$ AA	τ_i (ps)		0.21	1.48
0.13 eV	A_i (%)	0.5	78.3	21.2
$\parallel$ DA	τ_i (ps)		0.27	1.65
		Bleach		
	A_i (%)	0.5	78.2	21.3
	τ_i (ps)		0.21	1.48
0.70 eV $\parallel$ AA		Rise		
	B_i (%)		46.6	53.4
	τ_i (ps)		0.41	3.59
0.88 eV	A_i (%)	23.4	72.0	4.6
$\parallel$ DA	τ_i (ps)		0.27	1.65

generally longer as compared to the time resolution (~180 fs). Subsequently, the reflectivity sharply increases within ~400 fs due to the redshift of the A^- to A^- transition, which is caused by a transient decrease of the dimeric molecular displacements, as mentioned above. Noticeably, after the delayed increase of $\Delta R/R$, the prominent oscillations are observed, which is discussed later again.

On the basis of the above discussion, we analyzed the time profiles of $\Delta R/R$ at 0.13 eV [Eq. (1)] and $\Delta R/R$ at 0.70 eV [Eq. (2)] excluding oscillatory components by the following functions, respectively:

$$\frac{\Delta R(t_d)}{R} = \int_{-\infty}^{t_d} \left[A_0 + A_1 \exp\left(-\frac{t_d - t'}{\tau_1}\right) + A_2 \exp\left(-\frac{t_d - t'}{\tau_2}\right) \right] \exp\left(-\frac{t'^2}{\tau_0^2}\right) dt', \quad (1)$$

$$\frac{\Delta R(t_d)}{R} = -B_3(1) + B_4 \int_{-\infty}^{t_d} \left[1 - B_1 \exp\left(-\frac{t_d - t'}{\tau_1}\right) - B_2 \exp\left(-\frac{t_d - t'}{\tau_2}\right) \right] \exp\left(-\frac{t'^2}{\tau_0^2}\right) dt'. \quad (2)$$

τ_0 is the parameter related with the time resolution (180 fs) and is set to be 110 fs. Convolution integrals with the term $\exp(-t^2/\tau_0^2)$ corresponding to the time resolution are taken into account in Eqs. (1) and (2). In Eq. (1), τ_i and $A_i (i = 1,2)$ are the decay time and the amplitude of each exponential component, respectively. In Eq. (2), the first term shows the ultrafast bleaching component owing to the photogeneration and decay of photoinduced metallic states, which can be expressed by constant multiplication of Eq. (1). The second term in Eq. (2) corresponds to the delayed component owing to the photoinduced melting of the molecular dimerization. τ_i and $B_i (i = 1,2)$ are the rise time and the amplitude of each exponential component, respectively. $B_i (i = 3,4)$ is the amplitude of the first and second terms in Eq. (2). The experimental time profiles of $\Delta R/R$ at 0.13 and 0.70 eV were reproduced well, as shown by red solid lines in Figs. 8(a), 8(b), and 8(d). The parameter values are listed in Table I. In Fig. 8(d), each term in Eq. (2) was also shown by dashed and dashed-dotted lines.

B. Analyses of the coherent oscillations at low-temperature phase (10 K)

In Fig. 9(a), we show the oscillatory components $\Delta R_{osc}/R$ obtained by subtraction of the background rise and decay from $\Delta R/R$ shown in Fig. 8(d) [$E \parallel$ AA(DD) at 0.70 eV], which will include the information about the lattice dynamics. To obtain similar information about the lattice dynamics along the DA stack, we focus on the time profiles of $\Delta R/R$ associated with the A^- to D^+ transition at 0.88 eV (10 K), which is shown in Fig. 8(f). In Fig. 8(e), we also show the time profile of $\Delta R/R$ (294 K) at the A^- to D^+ transition energy (0.84 eV) for comparison. The coherent oscillation is not observed at 294 K but is observed only at 10 K [Fig. 8(f)]. In Fig. 9(b),

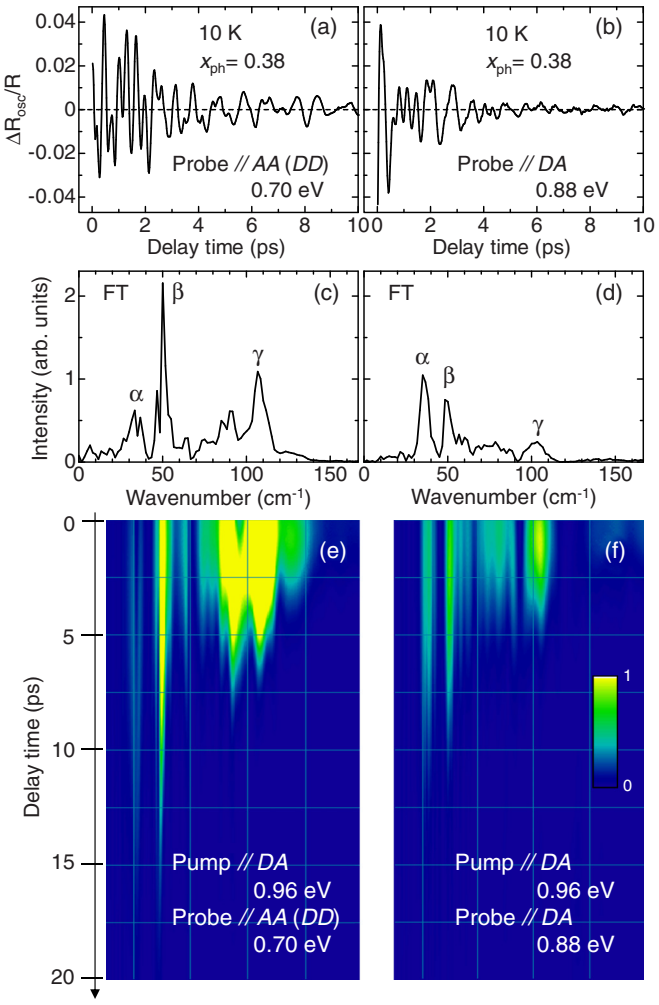

FIG. 9. (Color online) (a), (b) Oscillatory components $\Delta R_{osc}/R$ extracted from Figs. 8(d) ($E_{pr} \parallel$ AA) and 8(f) ($E_{pr} \parallel$ DA). (c), (d) Fourier power spectra of the oscillatory components shown in (a) and (b). (e), (f) Wavelet transform of the oscillatory components shown in (a) and (b).

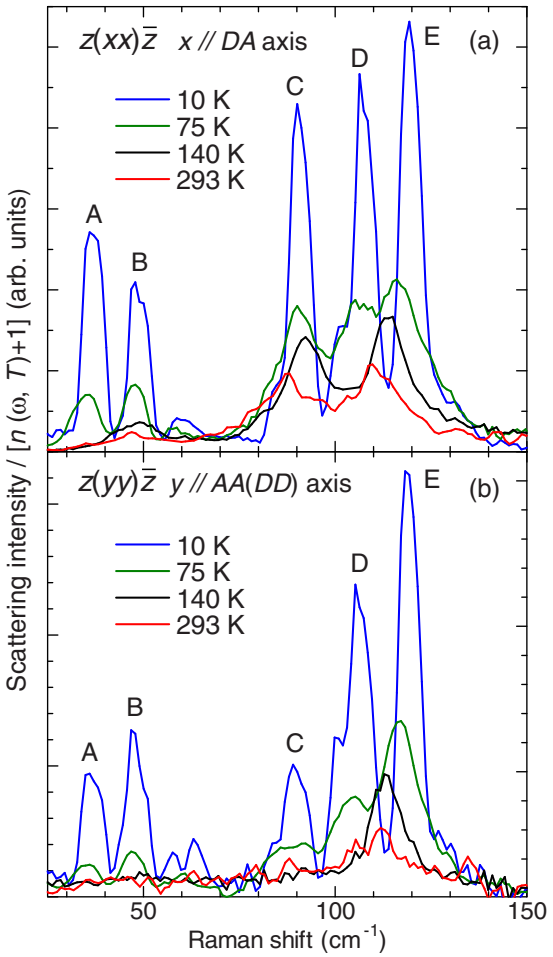

FIG. 10. (Color online) Temperature dependence of the polarized Raman spectra. The electric field of the incident light E_i and that of the scattering light E_s were polarized parallel to (a) the DA axis (x) and (b) the AA(DD) (y) axis, respectively. z indicates the direction of the incident light, which is perpendicular to the $(01\bar{1})$ plane The photon energy of the excitation light is 1.96 eV.

$\Delta R_{osc}/R$ for $E \parallel$ DA at 0.88 eV (10 K), which reflects the lattice dynamics along the DA stack, is presented.

From the time profiles shown in Figs. 9(a) and (b), we calculated the Fourier power spectra of the oscillatory components, which are shown in Figs. 9(c) and (d). Several coherent oscillations are observed for both $E \parallel$ AA and $E \parallel$ DA. The main bands are labeled α, β, and γ. We also performed wavelet analyses on the oscillatory components and obtained time-dependent Fourier power spectra, which are shown in Figs. 9(e) and 9(f) [32]. As can be seen, the frequencies of coherent oscillations are unchanged with time.

It is natural to consider that the coherent oscillations observed on $\Delta R/R$ are related to the release of lattice dimerizations by photoirradiation [9,16]. The fact that the coherent oscillations on $\Delta R/R$ are observed only below $T_C \sim$ 122 K [see Figs. 8(c)–8(f)] also supports this interpretation. To clarify the origin for the coherent oscillations, information on the phonon modes associated with the lattice dimerizations is necessary, which can be obtained from Raman spectroscopy. It is because in this type of low-dimensional molecular compound, a symmetry breaking of a lattice system should give rise to activations of lattice modes in Raman spectra. We measured the temperature dependence of polarized Raman spectra in M_2P-TCNQF$_4$ from 20 to 150 cm^{-1}, and the results are shown in Fig. 9. Polarizations of incident light E_i and that of the scattering light E_s were parallel to ($\parallel$) the DA axis (x) in Fig. 10(a) and the AA(DD) axis (y) in Fig. 10(b), respectively. z indicates the propagation direction of the incident light, which is perpendicular to the $(01\bar{1})$ plane. The photon energy of the excitation light is 1.96 eV. As the temperature increases, band E at ~120 cm^{-1} decreases in its intensity and broadens for both configurations, but it still has a finite intensity above T_C. Band C at ~90 cm^{-1} also decreases in its intensity and broadens with an increase of temperature for both configurations, and is almost deactivated above T_C for $z(yy)\bar{z}$. However, it has a finite intensity above T_C for $z(xx)\bar{z}$ Three bands labeled A, B, and D with frequencies of ~37, ~49, and ~107 cm^{-1} decrease gradually in intensity with an increase of temperature and are deactivated above T_C for both configurations. This indicates that bands A, B, and

D can be attributed to the lattice phonon modes activated in the low-temperature phase by dimerization, that is, the zone-boundary modes in the high-temperature phase, which are activated in the low-temperature lattice-dimerized phase by zone folding [16,17,33].

Here, we compare the observed coherent oscillations with Raman bands A–E. The frequencies of coherent oscillations labeled $\alpha(36\,\mathrm{cm}^{-1})$, $\beta(50\,\mathrm{cm}^{-1})$, and $\gamma(107\,\mathrm{cm}^{-1})$ [Figs. 9(c) and 9(d)] correspond well to the frequencies of the Raman bands A, B, and D, respectively. Therefore, the 36, 50, and 107 cm^{-1} modes are associated with the release of the dimeric molecular displacements. As shown in Figs. 9(c) and 9(d), coherent oscillations $\alpha(36\,\mathrm{cm}^{-1})$ have a smaller intensity in $E \parallel$ AA(DD) than in $E \parallel$ DA, whereas coherent oscillations $\beta(50\,\mathrm{cm}^{-1})$ and $\gamma(107\,\mathrm{cm}^{-1})$ have much a larger intensity in $E \parallel$ AA(DD) than in $E \parallel$ DA and β has the largest intensity in $E \parallel$ AA(DD). From these results, possible assignments of the coherent oscillations $\alpha(36\,\mathrm{cm}^{-1})$, $\beta(50\,\mathrm{cm}^{-1})$, and $\gamma(107\,\mathrm{cm}^{-1})$ are as follows: α is the longitudinal optical (LO) mode corresponding to the dimerization between D and A molecules, β is the LO mode corresponding to the dimerization between A molecules, and γ is the LO mode corresponding to the dimerization between D molecules.

C. Effect of the change in electronic structure via the phase transition on the photoresponse

In this section, first of all, we comment on how the difference between pump and probe absorption depths and the variation of probe absorption depths with photon energy affect the photoresponses of M_2P-TCNQF$_4$. At 10 K (294 K), the probe absorption depth for $E \parallel$ DA varies from 300 to 900 nm (from 750 to 3000 nm) by changing the energy from 0.5 to 0.1 eV in the inner-gap region, while that for $E \parallel$ AA varies from 300 to 1100 nm (from 500 to 800 nm) by changing the energy from 0.5 to 0.1 eV. For both directions, the probe absorption depths in this energy region are larger than the pump absorption depth 46 nm at 10 K (82 nm at 294 K). When metallic states are photogenerated, the probe absorption depths should be considerably decreased, so that the transient reflectivity spectra experimentally observed would not be so affected by the difference in the absorption depths for the pump and probe pulses. In the case when the excitation photon density is not so large or the carrier density is decreased at large t_d, however, the difference in the absorption depths for the pump and probe pulses might modify the transient reflectivity spectra. At 10 K, the photon-energy dependences of the probe absorption depths in the inner-gap region for $E \parallel$ DA and $E \parallel$ AA are similar. At 294 K, they are somewhat different, however, the difference is large only below 0.1 eV. Therefore, we consider that we can precisely discuss the relative difference of the reflectivity changes for $E \parallel$ DA and $E \parallel$ AA without serious corrections.

Next, we discuss how the change in the ground-state electronic structure via the phase transition is reflected in the photoresponse of M_2P-TCNQF$_4$ as observed. In the high-temperature phase, as shown in Fig. 2, transfer energies between the neighboring molecules for each stack are as follows: $t_{\mathrm{DA}}(= 67.1\ \mathrm{meV}) > t_{\mathrm{AA}}(= 43.1\ \mathrm{meV}) > t_{\mathrm{DD}}(= 29.3\ \mathrm{meV})$. t_{DD} is much smaller than t_{DA} and t_{AA} and the spectral weight of band c in the DD stacks is also much smaller than those of band a in the AA stacks and band b in the DA stacks. Therefore, we can consider that the observed photoresponses are mainly due to the photoinduced changes in the electronic states of the AA stack and the DA stack. Thus, we hereafter focus on the transfer energies t_{DA} and t_{AA}. t_{DA} is 1.6 times larger than t_{AA}. However, because of the alternative arrangement of D and A molecules, the effective bandwidth along the DA stack would be largely suppressed and smaller than that along the AA stack. It is natural to consider that the smaller effective bandwidth along the DA stack results in the smaller spectral weight of ε_2 for the DA stack in the inner-gap region [Figs. 4(a) and (b)]. Thus, a quasi-1D metallic state is generated by photoirradiation in the high-temperature phase.

On the other hand, in the low-temperature phase, the average value of t_{DA} considerably increases from 67.1 meV (294 K) to 91.1 meV (25 K), while the average value of t_{AA} is almost unchanged (43.1 meV at 294 K and 40.2 meV at 25 K); the averaged t_{DA} is more than two times larger than the averaged t_{AA}. In addition, regarding the degree of the dimerization δ_t

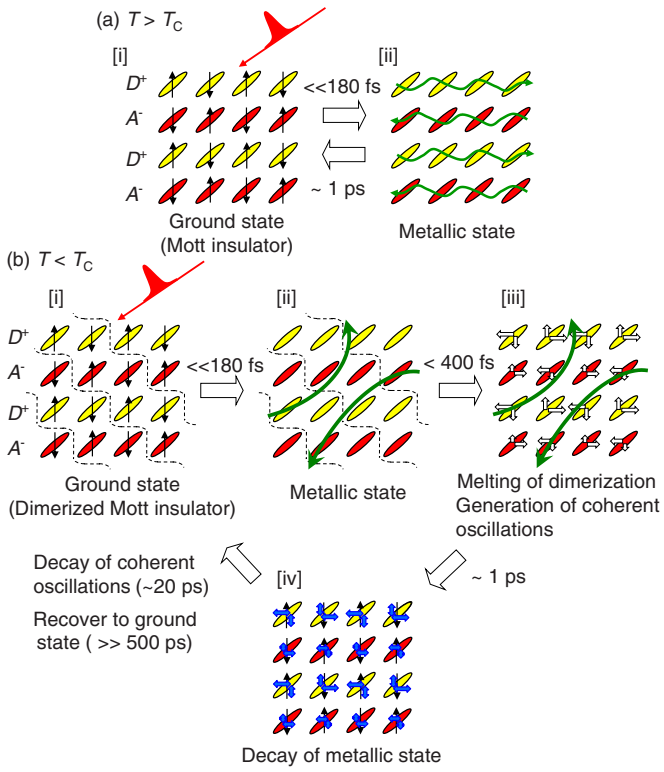

FIG. 11. (Color online) (a) Schematic view of photoinduced phenomena in the high-temperature phase (294 K). (i) Ground state of the Mott insulator with uniform AA(DD) and DA stacks. (ii) Quasi-1D photoinduced metallic state along AA(DD) stacks. (b) Schematic view of photoinduced phenomena in the low-temperature phase (10 K). (i) Ground state of the Mott insulator dimerized by the spin-lattice interaction. (ii) Quasi-2D photoinduced metallic state. (iii) Photoinduced melting of molecular dimerization and the generation of coherent oscillations. (iv) Decay of the photoinduced metallic state. The characteristic times deduced from the present study are shown in the figure.

defined as $(t_1 - t_2)/(t_1 + t_2)$ (t_1: intradimer transfer energy; t_2: interdimer transfer energy), $\delta_t = 0.485$ in the AA stack is much larger than $\delta_t = 0.095$ in the DA stack. Such a change in the DA and AA stack with respect to the transfer energy and dimerization causes a large enhancement of the effective bandwidth along the DA stack and suppression of that along the AA stack. It leads to a large enhancement of ε_2 along the DA stack and a slight suppression of ε_2 along the AA stack at $t_d = 0.1$ ps (10 K) in the inner-gap region [Figs. 6(a) and 6(b)]. This results in the photogeneration of a transient quasi-2D metallic state. Mixed-stack CT compounds consisting of DA stacks are usually insulators or semiconductors in the ground state. Therefore, the present observation of photoinduced metallization in the DA stack is quite intriguing, although the metallic state is transient and decays within 1 ps, as discussed in Sec. IV A.

Finally, on the basis of the results presented above, we summarize the dynamics for the photoinduced phase transition in M_2P-TCNQF$_4$ as shown in the scheme in Fig. 11. In the high-temperature phase (294 K), upon photoexcitation, a quasi-1D metallic state along the AA(DD) stack is generated within the time resolution (<180 fs) via purely electronic processes [Fig. 11(a)(ii)], and then decays rapidly within ~1 ps. In the low-temperature phase (10 K), on the other hand, a quasi-2D metallic state is formed by photoexcitation within the time resolution [Fig. 11(b)(ii)]. In the formation process of the metallic state, lattice dimerizations persist as shown in Fig. 11(b)(ii). Subsequently, photoinduced releases of lattice dimerizations occur within ~400 fs [Fig. 11(b)(iii)]. Simultaneously, the photogenerated metallic state exhibits ultrafast decay within ~1 ps, and several kinds of coherent oscillations due to the releases of dimerizations are generated [Figs. 11(b)(iii) and 11(b)(iv)]. Coherent oscillations decay within ~20 ps, and the system subsequently returns to the ground state (≫500 ps).

V. CONCLUSION

We have investigated photoinduced phase transitions in a two-dimensional Mott insulator M_2P-TCNQF$_4$ with strong anisotropy by applying femtosecond pump-probe reflection spectroscopy. This compound exhibits a structural and magnetic phase transition at 122 K below which two neighboring molecules are dimerized along both the AA(DD) ([100] direction) and DA ([111] direction) stacks. The results show that the two kinds of photoinduced phase transitions occur by irradiation of the femtosecond laser pulse. In the high-temperature lattice-uniform phase, we demonstrated that a quasi-one-dimensional metallic state along the AA(DD) stack can be induced by irradiation of a femtosecond laser pulse. In the low-temperature lattice-dimerized phase, upon photoirradiation, photoinduced metallization along the DA stack as well as the AA (DD) stack is initially realized because of the large enhancement of the effective bandwidth in the DA stack, which results in a quasi-two-dimensional metallic state. Mixed-stack CT compounds consisting of DA stacks are generally electrical insulators or semiconductors in the ground state. Such a dynamical metallization in the DA stack by photoirradiation has been demonstrated in the present study. Photoirradiation of M_2P-TCNQF$_4$ at low temperatures using a femtosecond laser pulse also stimulates the melting of lattice dimerization, which is accompanied by three kinds of coherent oscillations. These modes play important roles in the stabilization of the two-dimensional lattice-dimerized phase.

ACKNOWLEDGMENT

This work has been partly supported by a Grant-in-Aid for Scientific Research from the Japan Society for the Promotion of Science (No. 22740197) and the Ministry of Education, Culture, Sports, Science, and Technology in Japan (No. 20110005).

[1] For a review, see *Photoinduced Phase Transitions*, edited by K. Nasu (World Scientific, Singapore, 2004).
[2] For a review, see M. Gonokami and S. Koshihara, J. Phys. Soc. Jpn. **75**, 011001 (2006).
[3] F. Schmitt, P. Kirchmann, U. Bovensiepen, R. G. Moore, L. Rettig, M. Krenz, J.-H. Chu, N. Ru, L. Perfetti, D. H. Lu, M. Wolf, I. Fisher, and Z.-X. Shen, Science **321**, 1649 (2008).
[4] M. Eichberger, H. Schäfer, M. Krumova, M. Beyer, J. Demsar, H. Berger, G. Moriena, G. Sciaini, and R. J. D. Miller, Nature (London) **468**, 799 (2010).
[5] L. Stojchevska, I. Vaskivskyi, T. Mertelj, P. Kusar, D. Svetin, S. Brazovskii, and D. Mihailovic, Science **344**, 177 (2014).
[6] S. Koshihara, Y. Tokura, T. Mitani, G. Saito, and T. Koda, Phys. Rev. B **42**, 6853 (1990).
[7] S. Iwai, S. Tanaka, K. Fujinuma, H. Kishida, H. Okamoto, and Y. Tokura, Phys. Rev. Lett. **88**, 057402 (2002).
[8] E. Collet, M. H. Cailleau, M. B. Cointe, H. Cailleau, M. Wulff, T. Luty, S. Koshihara, M. Meyer, L. Toupet, P. Rabiller, and S. Techert, Science **300**, 612 (2003).
[9] H. Okamoto, Y. Ishige, S. Tanaka, H. Kishida, S. Iwai, and Y. Tokura, Phys. Rev. B **70**, 165202 (2004).
[10] S. Iwai and H. Okamoto, J. Phys. Soc. Jpn. **75**, 011007 (2006).
[11] H. Uemura and H. Okamoto, Phys. Rev. Lett. **105**, 258302 (2010).
[12] T. Miyamoto, K. Kimura, T. Hamamoto, H. Uemura, H. Yada, H. Matsuzaki, S. Horiuchi, and H. Okamoto, Phys. Rev. Lett. **111**, 187801 (2013).
[13] M. Chollet, L. Guerin, N. Uchida, S. Fukaya, H. Shimoda, T.Ishikawa, K. Matsuda, T. Hasegawa, A. Ota, H. Yamochi, G Saito, R. Tazaki, S. Adachi, and S. Koshihara, Science **307**, 86 (2005).
[14] H. Okamoto, H. Matsuzaki, T. Wakabayashi, Y. Takahashi, and T. Hasegawa, Phys. Rev. Lett. **98**, 037401 (2007).
[15] S. Wall, D. Brida, S. R. Clark, H. P. Ehrke, D. Jaksch, A. Ardavan, S. Bonora, H. Uemura, Y. Takahashi, T. Hasegawa, H. Okamoto, G. Cerullo, and A. Cavalleri, Nat. Phys. **7**, 114 (2011).
[16] H. Okamoto, K. Ikegami, T. Wakabayashi, Y. Ishige, J. Togo, H. Kishida, and H. Matsuzaki, Phys. Rev. Lett. **96**, 037405 (2006).
[17] K. Ikegami, K. Ono, J. Togo, T. Wakabayashi, Y. Ishige, H. Matsuzaki, H. Kishida, and H. Okamoto, Phys. Rev. B **76**, 085106 (2007).
[18] H. Uemura, H. Matsuzaki, Y. Takahashi, T. Hasegawa, and H. Okamoto, J. Phys. Soc. Jpn. **77**, 113714 (2008).

[19] H. Uemura, N. Maeshima, K. Yonemitsu, and H. Okamoto, Phys. Rev. B **85**, 125112 (2011).
[20] S. Iwai, K. Yamamoto, A. Kashiwazaki, F. Hiramatsu, H. Nakaya, Y. Kawakami, K. Yakushi, H. Okamoto, H. Mori, and Y. Nishio, Phys. Rev. Lett. **98**, 097402 (2007).
[21] Z. G. Soos, H. J. Keller, J. Queckborner, D. Wehe, and S. Flandoris, J. Chem. Phys. **74**, 5287 (1981).
[22] M. Meneghetti, A. Girlando, and C. Pecile, J. Chem. Phys. **83**, 3134 (1985).
[23] S. A. Bewick and Z. G. Soos, J. Phys. Chem. B **110**, 18748 (2006).
[24] T. Mori, A. Kobayashi, Y. Sasaki, H. Kobayashi, G. Saito, and H. Inokuchi, Bull. Chem. Soc. Jpn. **57**, 627 (1984).
[25] M. Ohkura, Y. Ishige, R. Sawada, H. Matsuzaki, Y. Nogami, H. Nishikawa, M. Yamashita, S. Horiuchi, and H. Okamoto, Phys. Rev. B **84**, 085136 (2011).
[26] M. J. Cohen, L. B. Coleman, A. F. Garito, and A. J. Heeger, Phys. Rev. B **10**, 1298 (1974).
[27] S. Iwai, M. Ono, A. Maeda, H. Matsuzaki, H. Kishida, H. Okamoto, and Y. Tokura, Phys. Rev. Lett. **91**, 057401 (2003).
[28] H. Matsuzaki, M. Iwata, T. Miyamoto, T. Terashige, K. Iwano, S. Takaishi, M. Takamura, S. Kumagai, M. Yamashita, R. Takahashi, Y. Wakabayashi, and H. Okamoto, Phys. Rev. Lett. **113**, 096403 (2014).
[29] H. Okamoto, T. Miyagoe, K. Kobayashi, H. Uemura, H. Nishioka, H. Matsuzaki, A. Sawa, and Y. Tokura, Phys. Rev. B **82**, 060513(R) (2010).
[30] H. Okamoto, T. Miyagoe, K. Kobayashi, H. Uemura, H. Nishioka, H. Matsuzaki, A. Sawa, and Y. Tokura, Phys. Rev. B **83**, 125102 (2011).
[31] H. Matsuzaki, W. Fujita, K. Awaga, and H. Okamoto, Phys. Rev. Lett. **91**, 017403 (2003).
[32] H. Suzuki, T. Kinjo, Y. Hayashi, M. Takemoto, and K. Ono, J. Acoust. Emiss. **14**, 69 (1996).
[33] H. Schaefer, V. V. Kabanov, and J. Demsar, Phys. Rev. B **89**, 045106 (2014).